

## Article

# 2D Monte Carlo Simulation of Cocrystal Formation Using Patchy Particles

Bogdan Rangelov \*  and Christo Naney 

Rostislav Kaischew Institute of Physical Chemistry, Bulgarian Academy of Sciences, 1113 Sofia, Bulgaria

\* Correspondence: rangelov@ipc.bas.bg

**Abstract:** Cocrystals of Active Pharmaceutical Ingredients (APIs) are an attractive therapeutic alternative to salt formations. However, due to the molecular scale processes involved, the earliest stages of cocrystal formation remain poorly understood. In this paper, some light is shed on the thermodynamics and kinetics of co-crystallization. Importantly, to mimic the molecular scale processes of cocrystal formation, we use 2D Monte Carlo simulations and a computational model with short-range attraction and a mixture of two types of patchy particles (PPs) monomers. Each type possesses four patches, grouped in two by two, and each couple of patches is characterized by its specific placement on the circumference of the monomer and corresponding patch strength (a strong and narrow or weak and wide interaction). The spatial placement of the patches on both PPs monomers (alternating periodically through 60 and 120 degrees and vice versa) selected by us shows the emergence of both rhombohedral (metastable) and trihexagonal (stable) Kagome-like structures. The Kagome-like structures are preceded by formation of two types of trimers involving strong bonds only, or mixed trimers of strong and weak bonds, the later serving as building blocks for the finally generated Kagome patchy cocrystal, after prolonged simulation times. The step-by-step process governing the cocrystal formation is discussed in detail, concerning the temperature interval, concentrations of PPs, the specific patch geometry and patch anisotropy as well. It is to be hoped that an understanding of the mechanisms of co-crystallization can help to control practical cocrystal synthesis and the possible phase transformations.

**Keywords:** cocrystal; patchy particles; phase transition

**Citation:** Rangelov, B.; Naney, C. 2D Monte Carlo Simulation of Cocrystal Formation Using Patchy Particles. *Crystals* **2022**, *12*, 1457. <https://doi.org/10.3390/cryst12101457>

Academic Editor: Nikos Ch. Karayiannis

Received: 13 September 2022

Accepted: 11 October 2022

Published: 15 October 2022

**Publisher's Note:** MDPI stays neutral with regard to jurisdictional claims in published maps and institutional affiliations.



**Copyright:** © 2022 by the authors. Licensee MDPI, Basel, Switzerland. This article is an open access article distributed under the terms and conditions of the Creative Commons Attribution (CC BY) license (<https://creativecommons.org/licenses/by/4.0/>).

## 1. Introduction

Due to the inherent stability of crystalline materials and the positive impact of the crystallization processes on purification and isolation of chemical substances, typically, crystalline drugs are preferred to amorphous solid forms. However, due to the poor solubility in water of many Active Pharmaceutical Ingredients (APIs), enhanced interest in multi-component crystalline materials has been seen because they enable better drug bioavailability; these materials enable tuning the physicochemical properties of a drug, such as solubility and hence bioavailability, permeability, hydration, color, compaction, and tableting [1]. Especially when the widely used salt formations are unable to provide adequate enhancement of drug bioavailability (or cannot be formed due to the absence of ionization sites), an attractive alternative for improving the said characteristics are cocrystals of APIs (for a rigorous description of APIs see [2,3]) and a pharmaceutically acceptable cocrystal former (which do not alternate the pharmacological behavior of the APIs); the cocrystals of APIs are very promising for increasing drugs' poor aqueous solubility, slow dissolution rate in biological fluids (and hence insufficient bioavailability) and insufficient chemical stability of amorphous drugs, which results from their relatively high moisture uptake.

Cocrystals are homogeneous stoichiometric compositions of two or more neutral molecular constituents bound together in the same crystal lattice—but not a mixture of

pure component crystalline phases. Cocrystals encompass many types of compounds, including clathrates (which are inclusion compounds in which the guest molecule is in a cage formed by the host molecule or by a lattice of host molecules). The cocrystals are neither solvates nor simple salts. The different components in the cocrystal are neutral in nature when compared to salts that have ionized components, the distinction being that the proton is shared between an acid and a base in cocrystals while it is transferred when forming salts. The components in the cocrystal exist in a definite stoichiometric molar ratio and assemble via non-covalent interactions, such as hydrogen bonds, ionic bonds,  $\pi$ - $\pi$  or van der Waals interactions between the different molecular species. The molecules in the cocrystal superstructure are held together by supramolecular synthons [4] that are basic structural units formed from the non-covalent interactions. Importantly, the cocrystals' constituent components form a novel crystalline structure, which possesses unique properties [5,6].

Due to cocrystals' applications in the pharmaceutical industry [7–9], there is an active cocrystal research during these past few decades. There are many approaches to synthesize cocrystals [10]. The most frequently used one is slow evaporation from solutions of cocrystal-components contained in stoichiometric relations. This method ensures formation of a small number of larger crystals (as opposed to a high number of smaller crystals produced by other methods). To produce co-crystals via solvent evaporation, 1:1 stoichiometric amounts of co-crystal components are dissolved usually, e.g., [11]. Similar is the process of cooling co-crystallization. Another effective approach for cocrystal formation is the reaction co-crystallization method. In contrast to solvent evaporation, in the reaction crystallization method supersaturation with respect to the cocrystal is generated by reactant dissolution. Usually the drug, which is the least soluble component, is dissolved in solutions of the highly soluble component, which is usually the conformer [12]. Used is also co-grinding the reactants in the presence of small quantities of organic solvents or water added to the reactants during grinding. Melt processes can also produce co-crystals.

To address physicochemical, biopharmaceutical, and mechanical properties and to expand solid form diversity of the API, drug development scientists are exploring diverse cocrystals. For instance, first-principles modeling was employed to explore the design space for co-crystallization of caffeine–glutaric acid [13]. To account for uncertainty and variability in starting concentration, seed loading and seeding temperature, the operating ranges of process parameters on larger scales were determined via Monte Carlo simulation. (However, to the best of authors' knowledge, the cocrystal formation per se is not mimicked by Monte Carlo simulations.) Finally, it is worth noting that cocrystals are also promising for the design and preparation of new explosives [14].

The literature on cocrystals is vast and constantly increasing. For recent reviews on co-crystals see [10,15,16]. A comprehensive book on the rational control of pharmaceutical cocrystals has also been published [17]. However, despite the long history of cocrystals study, spanning more than 160 years, no theory for crystallization of pharmaceutical cocrystals has been devised until now. Importantly, the process of co-crystallization imposes additional levels of complexity when considering APIs behavior in solution and during crystallization. For instance, it is noted in Ref. [16] that “the complexity of the thermodynamic landscape and the kinetics of co-crystallization offers fresh challenges which are not encountered in single component crystallization.” Therefore, both thermodynamics and kinetics of co-crystallization are considered in this paper.

Especially from an industrial perspective, there is an increased awareness of the need to understand the co-crystallization process in more details. However, due to the molecular scale of the processes involved, there is little fundamental understanding of what is happening in a solution as molecules interact and begin to form entities that eventually become crystals. Presently, chemical engineers in the pharmaceutical and chemical industries handle the transformation from the liquid to the solid state in an empirical fashion that is not based on rigorous thermodynamic or kinetic principles. This approach is limited as molecular details are omitted. For instance, although critical for

obtaining a cocrystal from solution, the role of a solvent in nucleation of cocrystals remains poorly understood [18]. (However, it is logical to suggest that changing the solvent will change the intermolecular interactions and enable cocrystal formation.)

In this paper, the theoretical consideration of co-crystallization is started by pointing out rules known from the kinetics of single component crystallization that also govern the co-crystallization process. Our aim is to contribute to elucidating the principles and the molecular-scale mechanisms of the co-crystallization process, imposing additional levels of understanding when considering APIs behavior in solution. With this end in view, different intermolecular interactions are assumed when modeling co-crystallization by 2D Monte Carlo simulation.

## 2. Theoretical Consideration of the Co-Crystallization Process

Importantly, co-crystallization is almost always a thermodynamically favorable process [19]. Evidently, it is favored by the high conformational entropy ( $S$ ) of the cocrystal. The famous Boltzmann equation renders the statistical definition of the entropy:

$$S = k_B \ln W \quad (1)$$

where  $W$  is the number of different ways in which the energy of the system can be achieved by rearranging the molecules among their available states, i.e., their different configurations. Especially for the cocrystals,  $W$ , and thus  $S$ , are much higher as compared with the corresponding values for one-component crystals. Recalling that the second law of thermodynamics states that the entropy of an isolated system always increases for a spontaneous (i.e., a naturally occurring) process, i.e.,  $\Delta S > 0$ , under properly selected conditions, the co-crystallization is a spontaneous process occurring due to a decrease in the system's free energy. Therefore, it does not need to be driven by an outside source of energy. This explains the relatively ready co-crystallization and cocrystal formation in many systems.

As concerns the kinetics of co-crystallization, it is feasible to suggest that the general rules established for the growth of one-component crystals also rule the co-crystallization. For a diffusion-limited crystal growth, the growth rate is written as:

$$R = \frac{dm}{dt} = \left( \frac{SD}{\delta_N} \right) (c_t - c_e) \quad (2)$$

where  $S$  is crystal surface,  $\delta_N$  is the thickness of the Nernst diffusion layer;  $c_t$  denotes the solute concentration (which can differ for the two components) at any crystal growth moment of time  $t$ , and  $c_e$  being solubility, i.e., the equilibrium concentration with respect to an "infinitely" large crystal (activity coefficients equal to unity are assumed usually).  $D$  [ $\text{cm}^2/\text{s}$ ] is diffusivity, which can also differ for the two components. Additionally, the rate of the face propagation normal to itself ( $R_f$ ) is proportional to the supersaturation,  $c_t - c_e$  [20]:

$$R_f = pv = p\beta_{st}\Omega(c_t - c_e) \quad (3)$$

where  $p$  is the surface step density and  $v$  is the propagation rate of a step on the crystal face;  $\beta_{st}$  is the kinetic coefficient for step propagation, and  $\Omega$  denotes the volume of the crystal building unit.

The rate  $v$  of step propagation during growth of the crystal is determined by the kink density ( $\rho/\lambda_k$ ) and the velocity  $v_k$  of kink propagation along the step:

$$v = \left( \frac{\rho}{\lambda_k} \right) v_k = \left( \frac{\rho^2}{\lambda_k} \right) (j_+ - j_-) \quad (4)$$

where  $\rho$  is a typical molecular size,  $\lambda_k$  is the average distance between the kinks, and  $j_+$  and  $j_-$  are the frequencies of molecular attachment to and detachment from a kink, respectively. Kaischew showed that the number density of kinks of the two components is proportional

to its molar part [21] (and on the temperature), but  $j_+$  and  $j_-$ ,  $c_t$  and  $D$  must be determined separately for each cocrystal component.

Importantly, to design cocrystal screening experiments, it is vital to understand how the cocrystals' bonding arise and how they form. The desirable physicochemical properties are based on an understanding of the intermolecular interactions, which dictate the molecular arrangement in the crystal lattice [22]. In plain language, knowledge of the intermolecular interactions and their effects on crystal packing are indispensable for the engineering of cocrystals with desired physical and chemical properties.

To give a plausible explanation of the co-crystallization, the method of slow evaporation from solutions of cocrystal components will be considered first. It is evident that the two cocrystal ingredients must have a similar solubility. (Otherwise, solely one of them will crystallize.) Though, (exactly) the same solubility of two different substances is hardly possible—in general, slightly different solubilities are preferred. Therefore, the critical supersaturation, which is needed for crystal nucleation of one or the other of the cocrystal components is reached for one of the components somewhat earlier than for the other [23]. Thus, the critical cocrystal nucleus should be formed, at least predominantly, from the molecules of the slightly less-soluble co-crystal component. Growing under diffusion limitations, the cocrystal nucleus exhausts the molecules of the same kind in its surrounding. Then, when the second cocrystal component overcomes the solubility threshold, the crystallization continues further with deposition of the second cocrystal component molecules on the existing crystal nucleus. Imaginably, the co-crystallization consists of repeated exhausting and enrichment of the two kinds of molecules. (In fact, periodic co-crystallization is observed by some of our Monte Carlo simulations—a work in progress which will be published elsewhere).

Secondly, for reaction co-crystallization, the mechanism of periodic precipitation resembles Liesegang patterning [24]—in both cases the deposited material is formed due to chemical reactions; the difference being only the appearance of void of deposition bands which are typical for the Liesegang patterning, which is missing in cocrystals. However, the consideration of co-crystallization is complicated even in the case of solution having two cocrystal components. In principle, the concentration on the boundary of the Nernst diffusion layer can be calculated by solving the following diffusion-reaction differential equations:

$$\frac{\partial a}{\partial t} = D_a \left( \frac{\partial^2 a}{\partial x^2} + \frac{\partial^2 a}{\partial y^2} + \frac{\partial^2 a}{\partial z^2} \right) - R(a) \quad (5)$$

$$\frac{\partial b}{\partial t} = D_b \left( \frac{\partial^2 b}{\partial x^2} + \frac{\partial^2 b}{\partial y^2} + \frac{\partial^2 b}{\partial z^2} \right) - R(b) \quad (6)$$

where  $a$  and  $b$  denote the concentrations of the two components, while  $D_a$  and  $D_b$  are the corresponding diffusion coefficients;  $R(a)$  and  $R(b)$  are the cocrystal growth rates for the corresponding component. Unfortunately, such sets of nonlinear partial differential equations cannot be treated by standard analytical methods—the only viable way is the application of numerical methods. Yet, numerical solution of such systems of equations is computationally demanding, and even nowadays—computationally prohibitive. Therefore, to treat the before mentioned scenario of the cocrystal formation, we use Monte Carlo simulations, based on two types of “protein-like” patchy particles and computational model based on the widely used PPs model proposed by Doye and co-workers [25].

### 3. Monte Carlo Simulations: Computational Model, Results, and Discussion

Up to date, Monte Carlo (MC) simulation has been used predominantly as an auxiliary tool for proper design of co-crystallization of practically interesting systems. For instance, to account for the limited solute diffusion velocity through the boundary layer, analytical solution of a simple model of the boundary layer was combined via an iterative process with the MC simulation of the interface [26]. However, direct investigations of cocrystal formation by using MC simulation are relatively rare [27]. Clathrate formation was simulated

most recently, using standard Metropolis MC simulations in the canonical ensemble with equally likely single-particle translation and rotation moves [28]. Self-assembly scenario in a 2D binary mixtures of patchy colloidal particles (PPs) with attractive patches where the two components are characterized by different numbers of patchy sites were studied by Doppelbauer et al. [29].

In this paper, we perform standard Metropolis [30] Monte Carlo (MC) simulations in the canonical (NVT) ensemble with (equally likely) single-particle translation and rotation moves (the so-called roto-translation moves). The latter permit the particles to bind together in a way that is consistent with the target structure, thus removing the possibility of competing forms and ensuring the kinetic accessibility of the target structure. While the attraction of our PPs depends on the relative orientation of the particles, simultaneously, they also interact with an isotropic core repulsion. The specificity encoded by patch positions, patch interaction selectivity, and restrictions on spatial orientations ensure PPs assembling into the desired structure. Because for directional interactions the computational effort is considerably enhanced with respect to particles with spherically symmetric interactions, we have restricted ourselves to a simple model, working in two dimensions and using patch interactions that are based on potentials proposed by Doye et al. [25]. The PPs we use in our simulations are represented by a monomer, the circumference of which is “decorated” with two pairs of patches (four patches in total for a monomer). The first pair of patches are “strong and narrow” (SN), while the second patches are “weak and wide” (WW). Thus, the patches are arranged on the monomer in a sequence SN-SN-WW-WW with given values of the degrees between each two consecutive patches. Here strong or weak refer to the amplitude of the patch-patch interaction, while narrow or wide define the geometrically span of the patches, namely the extent of the corresponding patch in degrees (or the so-called patchy width) along the monomer circumference. A reasonable ground to use strong and weak patches in our simulations is the nature of the hydrogen bonds—because of their strength and directionality, hydrogen bonds are particularly amenable to formation of cocrystals. The “strong” (or “conventional”) hydrogen bond includes (N–H–O), (O–H–O), (–N–H–N), and (O–H–N), which have energies 20–40 kJ mol<sup>−1</sup>, while the “weak” hydrogen bonds involves the –C–H–O and C–H–O=C, having energies 2–20 kJ mol<sup>−1</sup> [4]. Thus, the strong and weak attractive patches in our simulations resemble the supramolecular synthons.

Here we will use two types of patchy particles which will “generate” the building blocks of our patchy cocrystals. In both types of the PPs, the patches are arranged in a sequence SN-SN-WW-WW but with different values of the degrees between each two consecutive patches. PPs type I are constructed by angular distribution 60–120–60–120 (degrees), while in PPs type II the angular distribution is 120–60–120–60, see Figure 1.



**Figure 1.** Patchy particles type I (left) and patchy particles type II (right). Strong and narrow SN patches (deep blue) and weak and wide WW patches (light blue) are distributed for both types in a sequence SN-SN-WW-WW, but for PPs type I as 60–120–60–120 degrees, while for PPs type II as 120–60–120–60 degrees. The corresponding monomers are in red (type I) and gold (type II).

Having a lot in common, the two types of PPs presented in Figure 1 have a very important difference, which is illustrated in Figures 2 and 3. Both type I and type II can form their own metastable rhombohedral structures (see Figure 2a,b), even they can form a mixed rhombohedral cocrystal structure in a ratio of 1:1 (see Figure 2c). This mixed



rhombohedral building block could be realized with four WW-WW bonds, as shown in Figure 2c, or by four SN-SN bonds, too.

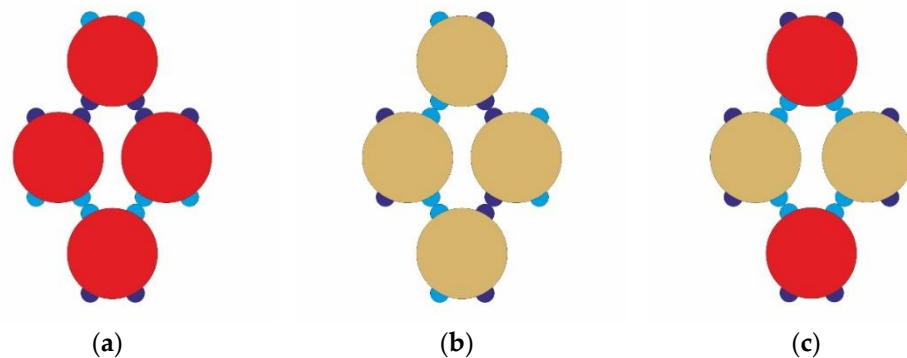


**Figure 2.** The three possible building blocks for the Rh-family structures: (a) Rh-phase formed from PPs type I only; (b) Rh-phase formed from PPs type II only (c) Mixed Rh-phase formed from PPs type I and type II.

Stable trimers can be formed solely by PPs of type I (see Figure 3a), while this is not possible for PPs of type II. However, it is possible for PPs of type II to be “included” in a mixed type of trimer in ratio 1:2 (see Figure 3b) and hence to develop Kagome cocrystal structure, which is expected to be more stable in a given temperature interval.

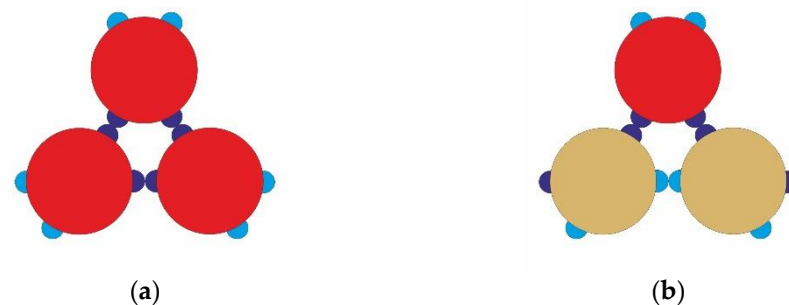


**Figure 3.** The two trimers which can be formed by PPs type I and type II: (a) trimer from PPs type I; (b) trimer formed by one PP type I and two PPs type II; Note that PPs type II cannot form solely a trimer.

Here we have to point out, that the mixed rhombohedral building block consists of two couples of PPs, connected by four identical bonds (this is the higher number of identical bonds in the so far presented building blocks from PPs type I and type II)—thus, this is rather a rare event, which explains why this mixed rhombohedral cocrystal phase is not well developed and monitored in our simulations.

Our computational model is based on the model introduced by Doye [25], slightly modified in order to include the two types of patches interactions—strong and narrow, and weak and wide. Patches of the same type interact via modulated 12-6 Lennard-Jones (LJ) pair potential with repulsive part for  $r_{ij} \leq \sigma$ , where no patch-patch interactions are available (excluded volume repulsion) and attractive part for  $r_{ij} > \sigma$ , which is multiplied by a number  $V_{Ang}$  between zero and one, depending on the mutual orientation of similar patches with respect to the inter-core vector connecting monomer  $M_i$  and monomer  $M_j$ —see Figure 4 (irrespective to type I or type II). Thus, the 12-6 LJ pair potential is modulated according to the mutual orientation of similar patches on monomers type I and type II. The value of  $V_{Ang}$  is calculated for every step for every two monomers according to

$$V_{Ang} = \exp \left[ - \frac{(\min \Theta_i^p)^2 + (\min \Theta_j^p)^2}{\Omega_p^2} \right], \text{ where index } p \text{ accounts for the like-type patches (SN-}$$

SN or WW-WW only),  $\Theta_i^p$  and  $\Theta_j^p$  are the angles enclosed by the core particle vector and the corresponding patch vector, and parameter  $\Omega_p$  gives the patchy extent in degrees (or, so called patchy width) along the particle circumference. In all simulations, the temperature is expressed in terms of the reduced temperature  $T^* = k_B T / \varepsilon_{SN-SN}$ , where  $\varepsilon_{SN-SN}$  is the amplitude of the SN-SN patches attractive interaction. We use the following values of the model parameters:  $\varepsilon_{SN-SN} = 1.0$ ;  $\varepsilon_{WW-WW} = 0.5$ ;  $\Omega_{WW-WW} = 10.0$ ;  $\Omega_{SN-SN} = 40.0$ .

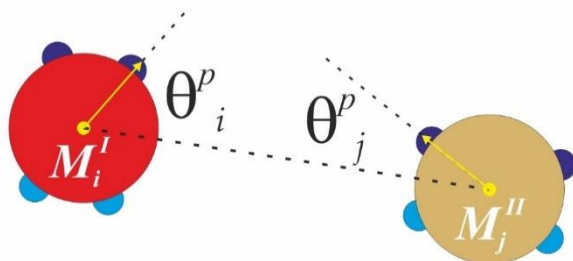


**Figure 4.** Minimal patchy angle between SN patches for monomer of type I ( $M_i$ ) and for monomer type II ( $M_j$ ). These angles are used to evaluate the modulated LJ interaction potential between the monomers.

Our task was to design a set of patchy particles, such that they can assemble into the targeted crystal structure. To do this, we used the following semi-empirical approach: Firstly, we drew the desired ordered structure and checked all possibilities that enable creating it by using patches with properties (geometry, interaction strength), needed to its assembly. In doing so, for each particle in our target structure we define patch vectors pointing at its nearest-neighboring particle; all particles of the same type have the same properties (number of patches, patch vectors, and all patch properties). Additionally, the MC simulation model selected by us [31] demonstrated structural flexibility (it allows two polymorphic forms but is not locked into a single type of crystalline lattice or packing mode), it was also used for simulation of the co-crystallization process.

As we will show, it is remarkable that a relatively simple “design” of PPs—with only two pairs of attractive patches, but having different strengths—enable 2D Monte Carlo simulation of co-crystallization. Altering patch positions only—from 60–120–60–120 (type I) to 120–60–120–60 (type II) degrees—the bonding interpatch energies remain the same (including in the cocrystals). This means that, because of the same number of uniform connections, the enthalpy is the same for all resulting crystal structures. Thus, the processes are dictated by entropy only, i.e., by the high cocrystal conformational entropy.

Separately, each of the two types of PPs shown in Figure 1 makes its “own” specific Rh-phase unit cell, characterized by different sorts of rhombuses (Figures 2a,b and 5a,b). So, separately, each PPs type is expected to make its own Rh-crystal phase, as shown on Figure 5. In fact, the PPs type I (60–120–60–120) generate a Rh-phase, which passing by through a polymorphic transition transforms into a Tri-hex (Kagome) lattice at specific temperature interval; and already beginning to make the Rh-structure, some PPs from type I start to create a relatively small number of stable trimers, formed solely by SN interactions (see Figure 3a). Details on this polymorph transition are given in [31]. In contrast, the PPs type II (120–60–120–60) cannot make its “own” stable trimers (and hence, no Kagome lattice from PPs type II could be built), but they generate their “own” Rh-phase only (see Figure 2b for the single structure unit and Figure 5b for the corresponding large crystal phase). Let’s point out that, strictly speaking, besides the Rh-phase, the PPs of type II can arrange in rings of six PPs. Formation of such rings is a rare event (because it requires very specific mutual in space and time orientation of type II monomers), and they are not stable either—when they reach the already grown Rh-phase they disintegrate into monomers, which are then incorporated sooner or later in the ridge of the growing Rh-phase.

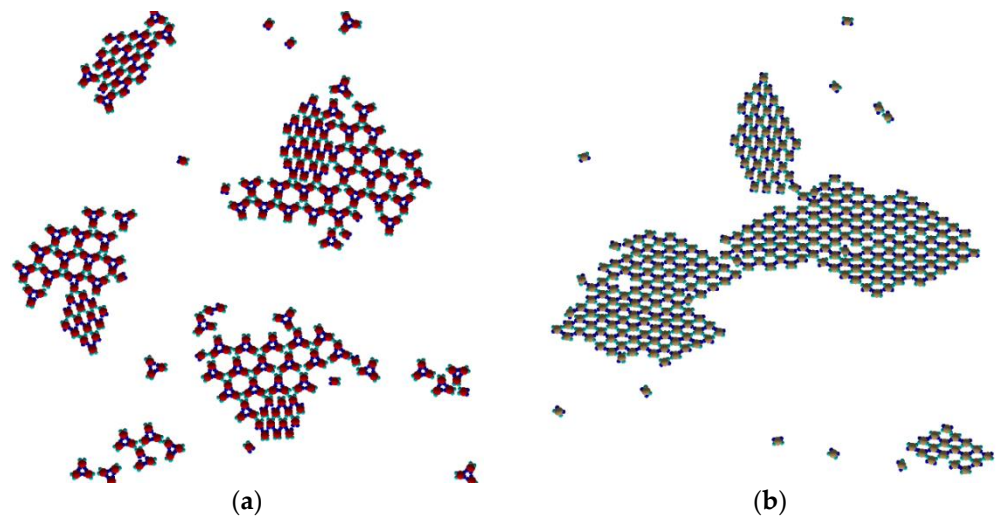


**Figure 5.** MC simulations at  $T^* = 0.10$  of pure PPs type I and PPs type II, with number density of 0.20: (a) metastable Rh and stable Kagome phase of PPs type I in time interval of their co-existence, for details see [31]; At prolonged simulation times only the Kagome phase survives. (b) (meta)stable Rh phase of PPs type II only. This is the only phase solely formed by this type of PPs.

Different is the situation when the two types of PPs are mixed-up in a starting composite “solution”. Under properly selected conditions of these composite “solutions”, the system of the two types of PPs evolve toward a Kagome like patchy cocrystal. Especially pronounced is the cocrystal Kagome lattice structure when the concentration ratio of the two PPs types differs from 1:1. Taking into account the structure of the mixed trimer (see Figure 3b) it is to be expected that solely Kagome cocrystal emerges when the concentration of PPs is one part of type I to two parts of type II. The sequence of steps of the Kagome cocrystal formation is shown by four snapshots in Figure 6, the corresponding energy of the system is shown in Figure 7, and one can identify the following key steps:

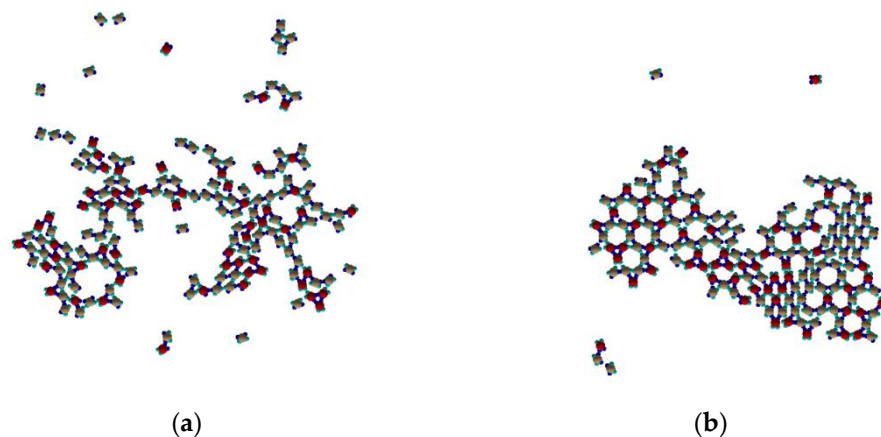


**Figure 6.** *Cont.*



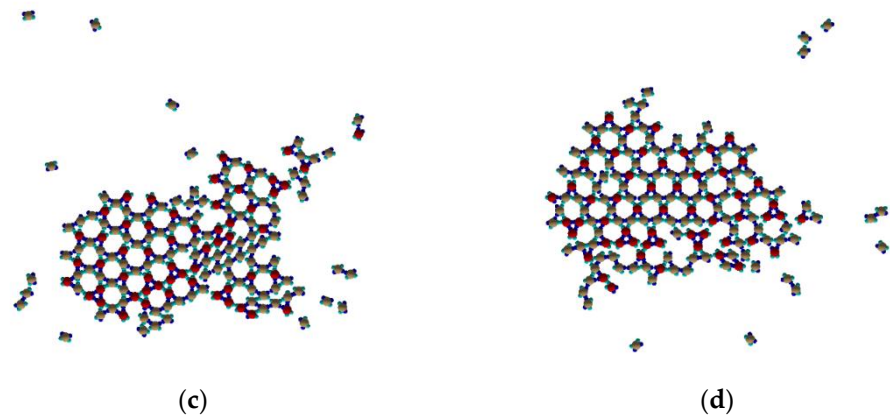


**Figure 6.** Sequence of steps of the Kagome cocrystal formation, concentration type I:type II = 1:2,  $T^* = 0.10$ : (a) after  $3.0E5$  MC steps; (b) after  $8.0E6$  MC steps; (c) after  $2.2E7$  MC steps; (d) after  $5.9E7$  MC steps.

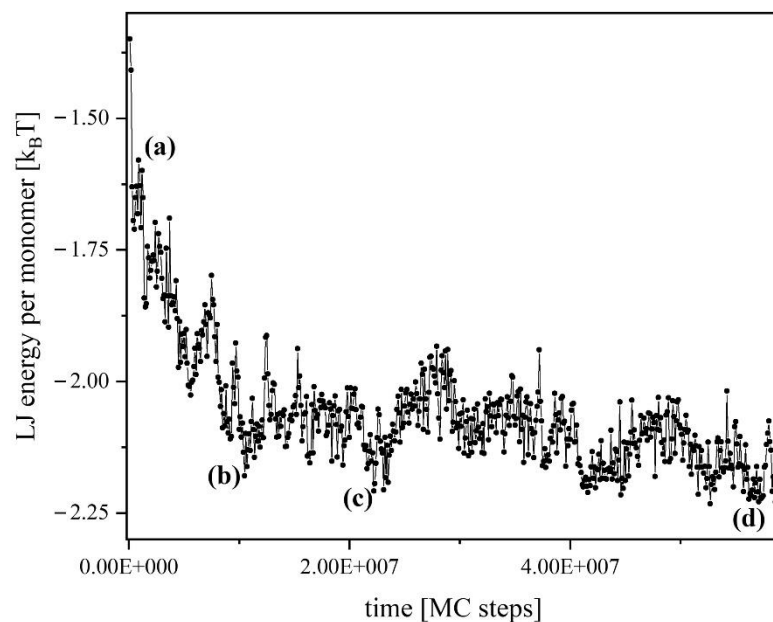


**Figure 7.** Evolution of the LJ interaction energy per monomer toward Kagome cocrystal structure. Energy corresponding to the snapshots configurations taken from Figure 6 (a–d) is indicated, too. The final Kagome structure (Figure 6d) is characterized by local energy minima ((d) on Figure 7).

Starting by randomly dispersed PPs type I and type II in ratio 1:2, shortly after the start of the simulations both of them begin to form the four possible building blocks, which could be “constructed” from PPs type I and type II, and already schematically shown in Figures 2 and 3—this is the Rh phase formed from PPs type I only, the Rh-phase formed from PPs type II only, the mixed Rh-phase building block, the Kagome phase trimer from PPs type I only and finally the most important Kagome mixed phase trimer from PPs type I and type II (see Figure 6a). Let us point out, that the Kagome mixed trimers prevail in number over the “pure” type I trimers, and this is due to the chosen ratio 1:2 of the monomers. As it was shown in [31], the Rh-phase type I is not stable and it “releases” monomers type I, which are subsequently “catch” by monomers type II and thus continue to form the mixed phase trimers (see Figure 6b), which begin to aggregate in Kagome cocrystal domains. This corresponds to a local minima of the system energy (see Figure 7). Figure 6c shows further development of the Kagome cocrystal by almost merging together the small cocrystal domains and repetitively creating and breaking bonds toward an increasingly stable and

a less defect structure. Because of the relative low number of “pure” type I trimers, they are not able to “built” their own “pure” Kagome lattice and they are incorporated into the growing cocrystal. Mixed Rh-phase cocrystal small domains are presented, too.

The final cocrystal Kagome structure is shown in Figure 6d, which possesses minimal system energy. Of course, due to the inevitable presence of the stable type I trimers, the cocrystal presents some defects, especially at its edges. Just one building block of the mixed Rh-phase is presented in Figure 6d, too. This is due to the fact that such a complex is a very rare event to be formed, as it requires four identical bonds to be properly oriented.

Keeping the temperature  $T^* = 0.10$ , concentrations different from of 1:2 cannot produce “large” periodic cocrystal Kagome or even Rh-like structures (see Figure 8). One can find several domains, consisting of rhombohedral-like placement of PPs type I and type II, without defined periodicity, and Kagome-like placement of both type trimers, also without defined periodicity.

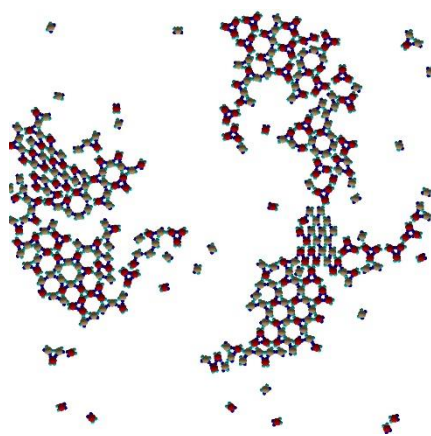


**Figure 8.** Growth structure from concentration of monomers type I:type II = 1:1,  $T^* = 0.10$  after  $5.9E7$  MC steps—several different domains with rhombohedral and Kagome like placement of the PPs, but without defined periodicity.

In conclusion, controlling the concentration ratio of the two PPs types at fixed  $T^* = 1.0$ , it is possible to simulate stable Kagome structures, which are of enhanced interest recently, e.g., [32]. However, besides the “solution” composition, the cocrystal stability strongly depends on temperature,  $T^*$ . Recall that  $T^*$  is interrelated with the interparticle bonding energy: evidently, the higher  $T^*$  corresponds to a relatively lower intermolecular bonding in the cocrystals. Practically important is that the weakened intermolecular bonding in cocrystals results in higher water-solubility, and hence in higher bioavailability of pharmaceutical cocrystals. Therefore, the dependence of the Kagome cocrystal stability on  $T^*$  was checked carefully. It turns out that “optimal” are temperatures in a very narrow interval at approximately  $T^* = 0.10$ .

At temperatures below 0.10 (see Figure 9a) Rh-phase like placement of PPs is dominant without defined periodicity. Beside it, some type I and mixed trimers, and some mixed ring structures as well can be identified. At temperatures slightly above 0.10 (see Figure 9b) the dominant structures are type I and mixed trimers. At such “elevated” temperature the trimers are not able to form stable Kagome cocrystal.

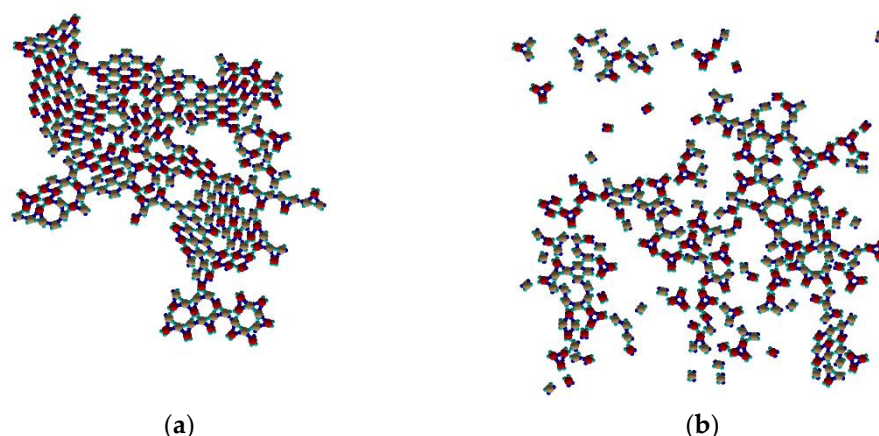


**Figure 9.** Growth structure from concentration of monomers type I: type II = 1:2, after 5.9E7 MC steps: (a)  $T^* = 0.08$ ; (b)  $T^* = 0.11$ .

#### 4. Conclusions

Understanding the mechanisms of co-crystallization can help to control cocrystal synthesis and possible phase transformations. In this work, the problem is considered theoretically and by 2D Monte Carlo simulation. The theoretical and simulation approaches enable elucidation of some molecular-scale processes that can enable co-crystallization: The simulation of the cocrystal formation has revealed what properties the molecules should possess to form targeted cocrystal structures (in the case under consideration, rhombohedral and/or Kagome lattices). Moreover, the observation that the composition of the Kagome structures corresponds exactly to the particle ratio in the output mixture can give practical clues for synthesizing cocrystals. Our hope is that this study may help in the efforts to produce cocrystals of APIs.

**Author Contributions:** Conceptualization, B.R. and C.N.; methodology, B.R. and C.N.; software, B.R.; validation, B.R. and C.N.; formal analysis, B.R. and C.N.; investigation, B.R. and C.N.; writing—B.R. and C.N.; writing—review and editing, B.R. and C.N.; visualization, B.R.; supervision, B.R. and C.N. All authors have read and agreed to the published version of the manuscript.

**Funding:** This research received no external funding.

**Data Availability Statement:** Not applicable.

**Acknowledgments:** B.R. acknowledges the support by the European Regional Development Fund within the OP Science and Education for Smart Growth 2014–2020, Project CoE National center for mechatronics and clean technologies, No.BG05M2OP001-1.001-0008, and Project INFRAMAT—part of the Bulgarian National Roadmap for Scientific Infrastructure, supported by the Ministry of Education and Science.

**Conflicts of Interest:** The authors declare no conflict of interest.

#### References

1. Bolla, G.; Sarma, B.; Nangia, A.K. Crystal Engineering of Pharmaceutical Cocrystals in the Discovery and Development of Improved Drugs. *Chem. Rev.* **2022**, *122*, 11514–11603. [\[CrossRef\]](#) [\[PubMed\]](#)
2. Vioglio, P.G.; Chierotti, M.R.; Gobetto, R. Pharmaceutical aspects of salt and cocrystal forms of APIs and characterization challenges. *Adv. Drug Deliv. Rev.* **2017**, *117*, 86–110. [\[CrossRef\]](#)
3. Steed, J.W. The role of co-crystals in pharmaceutical design. *Trends Pharmacol. Sci.* **2013**, *34*, 185–193. [\[CrossRef\]](#) [\[PubMed\]](#)
4. Desiraju, G.R. Supramolecular Synthons in Crystal Engineering—A New Organic Synthesis. *Angew. Chem. Int. Ed.* **1995**, *34*, 2311–2327. [\[CrossRef\]](#)
5. Almarsson, Ö.; Zaworotko, M.J. Crystal engineering of the composition of pharmaceutical phases. Do pharmaceutical co-crystals represent a new path to improved medicines? *ChemComm* **2004**, 1889–1896.
6. Aitipamula, S.; Banerjee, R.; Bansal, A.K.; Biradha, K.; Cheney, M.L.; Choudhury, A.R.; Desiraju, G.R.; Dikundwar, A.G.; Dubey, R.; Duggirala, N.; et al. Polymorphs, Salts, and Cocrystals: What's in a Name? *Cryst. Growth Des.* **2012**, *12*, 2147–2152. [\[CrossRef\]](#)

7. Miroshnyk, I.; Mirza, S.; Sandler, N. Pharmaceutical co-crystals—an opportunity for drug product enhancement. *Expert Opin. Drug Deliv.* **2009**, *6*, 333–341. [[CrossRef](#)] [[PubMed](#)]
8. Childs, S.L.; Zaworotko, M.J. (Eds.) The Reemergence of Cocrystals: The Crystal Clear Writing is on the Wall Introduction to Virtual Special Issue on Pharmaceutical Cocrystals. *Cryst. Growth Des.* **2009**, *9*, 4208–4211. [[CrossRef](#)]
9. Hadjittofis, E.; Isbell, M.A.; Karde, V.; Varghese, S.; Ghoroi, C.; Heng, J.Y.Y. Influences of Crystal Anisotropy in Pharmaceutical Process Development. *Pharm. Res.* **2018**, *35*, 100. [[CrossRef](#)] [[PubMed](#)]
10. Karimi-Jafari, M.; Padrela, L.; Walker, G.M.; Croker, D.M. Creating Cocrystals: A Review of Pharmaceutical Cocrystal Preparation Routes and Applications. *Cryst. Growth Des.* **2018**, *18*, 6370–6387. [[CrossRef](#)]
11. Bathori, N.B.; Lemmerer, A.; Venter, G.A.; Bourne, S.A.; Caira, M.R. Pharmaceutical Co-crystals with Isonicotinamide—Vitamin B3, Clofibric Acid, and Diclofenac—and Two Isonicotinamide Hydrates. *Cryst. Growth Des.* **2011**, *11*, 75–87. [[CrossRef](#)]
12. Rodríguez-Hornedo, N.; Nehm, S.J.; Seefeldt, K.F.; Pagán-Torres, Y.; Falkiewicz, C.J. Reaction Crystallization of Pharmaceutical Molecular Complexes. *Mol. Pharm.* **2006**, *3*, 362–367. [[CrossRef](#)]
13. Yu, Z.Q.; Chow, P.S.; Tan, R.B.H. Design Space for Polymorphic Co-crystallization: Incorporating Process Model Uncertainty and Operational Variability. *Cryst. Growth Des.* **2014**, *14*, 3949–3957. [[CrossRef](#)]
14. Chen, P.; Zhang, L.; Zhu, S.; Cheng, G. Theoretical study of BTF/TNA cocrystal: Effects of hydrostatic pressure and temperature. *Defence Technol.* **2015**, *11*, 132–139. [[CrossRef](#)]
15. Malamataris, M.; Ross, S.A.; Douroumis, D.; Velaga, S.P. Experimental cocrystal screening and solution based scale-up cocrystallization methods. *Adv. Drug Deliv. Rev.* **2017**, *117*, 162–177. [[CrossRef](#)] [[PubMed](#)]
16. Pawar, N.; Saha, A.; Nandan, N.; Parambil, J.V. Solution Cocrystallization: A Scalable Approach for Cocrystal Production. *Crystals* **2021**, *11*, 303. [[CrossRef](#)]
17. Wouters, J.; Quéré, L. (Eds.) *Pharmaceutical Salts and Co-Crystals*; Royal Society of Chemistry: Cambridge, UK, 2012.
18. Vishweshwar, P.; McMahon, J.A.; Bis, J.A.; Zaworotko, M.J. Pharmaceutical co-crystals. *J. Pharm. Sci.* **2006**, *95*, 499–516. [[CrossRef](#)] [[PubMed](#)]
19. Taylor, C.R.; Day, G.M. Evaluating the energetic driving force for cocrystal formation. *Cryst. Growth Des.* **2018**, *18*, 892–904. [[CrossRef](#)] [[PubMed](#)]
20. Chernov, A.A. Protein crystals and their growth. *J. Struct. Biol.* **2003**, *142*, 3–21. [[CrossRef](#)]
21. Kaischew, R. Über die Anwendung der Methode der mittleren Abtrennungsarbeiten in der Theorie der Kristallkeimbildung und des Kristallwachstums. *Fortschr. Mineral.* **1960**, *38*, 7–21.
22. Ross, S.A.; Lamprou, D.A.; Douroumis, D. Engineering and manufacturing of pharmaceutical co-crystals: A review of solvent-free manufacturing technologies. *Chem. Commun.* **2016**, *52*, 8772–8786. [[CrossRef](#)]
23. Thayyil, A.R.; Juturu, T.; Nayak, S.; Kamath, S. Pharmaceutical Co-Crystallization: Regulatory Aspects, Design, Characterization, and Applications. *Adv. Pharm. Bull.* **2020**, *10*, 203–212.
24. Liesegang, R.E. Ueber einige Eigenschaften von Gallerten. *Nat. Wochenschr.* **1896**, *11*, 353–362.
25. Doye, J.P.K.; Louis, A.A.; Lin, I.C.; Allen, L.R.; Noya, E.G.; Wilber, A.W.; Kok, H.C.; Lyus, R. Controlling crystallization and its absence: Proteins, colloids and patchy models. *Phys. Chem. Chem. Phys.* **2007**, *9*, 2197–2205. [[CrossRef](#)] [[PubMed](#)]
26. Saska, M. Binary crystal growth from solution. Monte Carlo simulation of the terephthalic acid-4-carboxybenzaldehyde. *Part. Sci. Technol.* **1986**, *4*, 409–417. [[CrossRef](#)]
27. Bommineni, P.K.; Punathanam, S.N. Molecular simulation of homogeneous crystal nucleation of AB2 solid phase from a binary hard sphere mixture. *J. Chem. Phys.* **2017**, *147*, 064504. [[CrossRef](#)] [[PubMed](#)]
28. Tracey, D.F.; Noya, E.G.; Doye, J.P.K. Programming patchy particles to form complex periodic structures. *arXiv* **2019**, arXiv:1909.10601v1. [[CrossRef](#)] [[PubMed](#)]
29. Doppelbauer, G.; Bianchi, E.; Kahl, G. Self-assembly scenarios of patchy colloidal particles in two dimensions. *J. Phys. Condens. Matt.* **2010**, *22*, 104105. [[CrossRef](#)] [[PubMed](#)]
30. Metropolis, N.; Rosenbluth, A.W.; Rosenbluth, M.N.; Teller, A.H.; Teller, E.J. Equation of State Calculations by Fast Computing Machines. *Chem. Phys.* **1953**, *21*, 1087.
31. Ranguelov, B.; Nanev, C. 2D Monte Carlo Simulation of Patchy Particles Association and Protein Crystal Polymorph Selection. *Crystals* **2019**, *9*, 508. [[CrossRef](#)]
32. Jing, Y.; Heine, T. Making 2D topological polymers a reality. *Nat. Mater.* **2020**, *19*, 823–824. [[CrossRef](#)]